An assessment of mode-coupling and falling-friction mechanisms in railway curve squeal through a simplified approach

Bo Ding[1], Giacomo Squicciarini[1,*], David Thompson[1], Roberto Corradi[2]

1: Institute of Sound and Vibration Research, University of Southampton
Highfield, Southampton, SO17 1BJ, UK

2: Politecnico di Milano, Dipartimento di Meccanica
Via La Masa 1, Milano, Italy

Published in Journal of Sound and Vibration, 423, 2018, 126–140.
https://doi.org/10.1016/j.jsv.2018.02.048

Bo Ding, Giacomo Squicciarini, David Thompson, Roberto Corradi, An assessment of mode-coupling and falling-friction mechanisms in railway curve squeal through a simplified approach, Journal of Sound and Vibration, 423, 2018, 126–140.

*: Corresponding author: Giacomo Squicciarini, email: G.Squicciarini@soton.ac.uk

Abstract

Curve squeal is one of the most annoying types of noise caused by the railway system. It usually occurs when a train or tram is running around tight curves. Although this phenomenon has been studied for many years, the generation mechanism is still the subject of controversy and not fully understood. A negative slope in the friction curve under full sliding has been considered to be the main cause of curve squeal for a long time but more recently mode coupling has been demonstrated to be another possible explanation. Mode coupling relies on the inclusion of both the lateral and vertical dynamics at the contact and an exchange of energy occurs between the normal and the axial directions. The purpose of this paper is to assess the role of the mode-coupling and falling-friction mechanisms in curve squeal through the use of a simple approach based on practical parameter values representative of an actual situation. A tramway wheel is adopted to study the effect of the adhesion coefficient, the lateral contact position, the contact angle and the damping ratio. Cases corresponding to both inner and outer wheels in the curve are considered and it is shown that there are situations in which both wheels can squeal due to mode coupling. Additionally, a negative slope is introduced in the friction curve while keeping active the vertical dynamics in order to analyse both mechanisms together. It is shown that, in the presence of mode coupling, the squealing frequency can differ from the natural frequency of either of the coupled wheel modes. Moreover, a phase difference between wheel vibration in the vertical and lateral directions is observed as a characteristic of mode coupling. For both these features a qualitative comparison is shown with field measurements which show the same behaviour.

Keywords: curve squeal, railway noise, mode coupling, friction induced vibration

1 Introduction

Curve squeal noise is a high amplitude tonal noise, which often occurs when a train or tram negotiates a tight curve. Curve squeal is considered to be generated from the self-excited vibration of the wheel in one of its natural modes [1]. Although it has been studied for several decades, the mechanism behind curve squeal is still the subject of some controversy. Two main causes have been proposed and discussed in the literature: negative slope in the friction coefficient and ‘mode coupling’.

When a rail vehicle negotiates a sharp curve the leading wheelset exhibits a considerable yaw angle relative to the running direction, leading to a lateral sliding velocity at the wheel/rail contact [2]. The sliding velocity normalised by the running velocity is termed the creepage and has components in all three directions (two translations and one rotation) with each component giving rise to a creep force [3]. The adhesion coefficient is the ratio between the force in any of these directions and the normal force. This increases from zero with increasing creepage until it reaches saturation, at which point there is slip in the whole contact area and gross sliding occurs [4]. In some cases, for large creepages, the adhesion coefficient can decrease with further increase of creepage and the friction-creepage curve can thereby exhibit a negative slope [5].

Rudd [6] proposed that the main mechanism for the occurrence of squeal noise is due to stick-slip motion induced by the wheel lateral sliding. Rudd showed that a decrease of friction force with increasing sliding velocity results in a negative damping effect, which then feeds energy into the system. Oscillations grow up to a limit cycle defined by the non-linearities in the creep forces. This falling friction mechanism has been accepted and adopted by many researchers, and several subsequent authors extended Rudd's model further. Fingberg [7] developed a time-domain squeal model, which consists of a finite element model of the wheel, a dynamic model of the track and a boundary element model for the sound radiation. Périard [8] extended Fingberg's model by including the vehicle curving behaviour. Heckl and Abrahams [9, 10] developed simple models in both the frequency domain and time domain. De Beer et al. [11] developed a model for squeal noise in the frequency domain, which was the first to include the variation of the normal contact force. However, although this feature can potentially introduce mode-coupling, it was not considered by the authors. Huang [12] extended de Beer's model to include all possible degrees of freedom in the wheel/rail contact. A further extension of this model was developed by Squicciarini et al. [13] to study the effect of two-point contact in a frequency domain approach. Chiello et al. [14] also considered normal contact dynamics. They pointed out that the asymmetry of the stiffness matrix, introduced by the influence of the normal load on the friction force, could lead to mode coupling and could be a different source of instability. Nevertheless, in their results this mechanism was only found to occur with a large lateral offset of the contact point.

Several laboratory measurements of squeal noise and friction behaviour have been performed on roller rigs and most of them have found the presence of a falling friction characteristic

with increased sliding velocity [11, 15-19], thus supporting the role of the original mechanism proposed by Rudd [6]. An exception is in the results measured on the rig adopted by Koch et al. [20] and by Collette [21]; in this case no negative slope was observed. Collette [21] pointed out that the vertical dynamics could play an important role in generating squeal in the case of a constant friction coefficient.

More recently it has been highlighted that squeal can still exist even under a constant friction condition; for this, coupling between different wheel modes has been proposed as an important mechanism. This phenomenon, also known in other contexts as flutter, results in instability at a frequency which is normally between those of the two coupled modes. In such a situation vertical and lateral vibrations exhibit a phase difference and can be characterised by beating [22]. In the transient curve squeal analysis carried out by Brunel et al. [23], it was found that the instability was due to the coupling of the normal and lateral dynamics of the wheel. Glocker et al. [24] used a constant friction coefficient in their model, and showed coupling between one axial mode and two radial modes. Pieringer [25] developed a time-domain squeal model in the case of a constant friction coefficient.

Field measurements of squeal noise have also been carried out by a number of researchers [5]. It was found that the occurrence of curve squeal was more frequent on the inner wheel [1, 24, 26-28]; however the outer wheel was also found to squeal in some cases [27, 29]. It was observed in [28], for a case involving squeal of freight vehicles, that the squealing frequency lay between two of the wheel's natural frequencies and this could be explained by assuming mode coupling between radial and circumferential modes. Additionally, some observations were reported by Jiang et al. in [30] showing that mode coupling could possibly exist in some curves that were monitored, again for freight wagons. Jiang et al. showed that vertical and lateral accelerations of the rail exhibited a phase difference and were characterised by beating. Both are typical features of mode coupling [22]. In [24], some frequency shift was observed but it was attributed to the Doppler Effect. In [27], for squeal noise from a tram, a frequency shift was found between the squealing frequency and the wheel natural frequency; one axial mode and one radial mode were found in the vicinity of the squealing frequency but no investigation was made into the possible role of mode coupling. For this reason these measured data from the tram are re-analysed in this paper to allow a qualitative comparison with the model developed here. Data were collected over a three-year period by Jiang et al. [31] using a wayside condition monitoring system in a curve with 300 m radius. It was found that freight trains generated more severe squeal noise than passenger trains and the likelihood

of squeal increased with angle of attack but it was found that even at large angles not every wheel squealed.

In investigating the mechanisms at the heart of curve squeal, both test rigs and field measurements have their own difficulties and limitations. Test rigs have been used to measure friction curves on several occasions but their dynamic behaviour is different compared with the one at full scale in traffic. Usually field measurements of squeal provide sound or vibration data whereas friction measurements directly associated with squeal are not present in the literature. Adhesion curves measured in the field are usually determined for traction and not for lateral creepage [5]. In both test rig and field measurements it would not be easily possible to distinguish in the measured data between mode coupling and falling friction unless some characteristic features of these mechanisms can be found in the measured results.

The purpose of this paper is to assess the respective roles of the mode-coupling and falling-friction instability mechanisms in curve squeal through the use of a simple approach. This approach is based on Hoffmann's model [22] with two modes applied to curve squeal using parameter values from a tramway wheel.

The two-mode model is introduced in Section 2. Different pairs of modes from a tramway wheel are adopted; these cases are described in Section 3. A parametric study is performed in Section 4 using a frequency-domain version of the two-mode model with practical parameter values representative of the tram wheel. An analysis of time-domain simulations of wheel vibration based on the same two-mode model is presented in Section 5, in particular to investigate the phase difference between the response in the normal and tangential directions. Finally in Section 6 wheel vibration measurements of this squealing tram wheel [27] are analysed and qualitatively compared with the model to identify the main features of the instability mechanisms from field measurement data.

2 A reduced two-mode model for curve squeal

2.1 Friction model

To compare the effects of the negative-slope and mode-coupling phenomena in this paper, both a falling characteristic and constant friction are considered. To calculate the contact force, the FASTSIM algorithm developed by Kalker [32] is adopted for values of creepage up to saturation. After saturation, the heuristic model of Huang [12] is adopted for the case of

falling friction. Figure 1 shows the adhesion-creepage curve obtained for the example parameters listed in Table 1. The values given in this table are arbitrary but realistic for actual conditions and are used as the starting point for the studies presented below. The dimensions of the contact patch (a and b in Table 1) are obtained from the actual geometry of the wheel analysed (see Section 3) and the preload applied. The rail head is assumed to have a transverse radius of 0.226 m. It can be seen from Figure 1 that the adhesion coefficient increases (in magnitude) from zero, until it saturates at the Coulomb friction μ_0. After saturation, the friction can remain constant or have a falling trend.

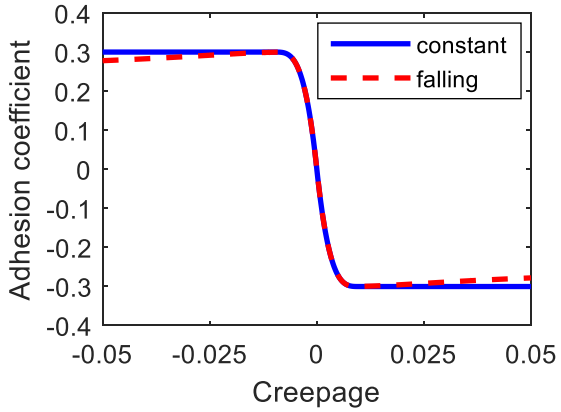

Figure 1. Adhesion coefficient with or without falling part based on parameters in Table 1.

Table 1. Parameters used for creep force curves

Description and Name	Value	Units
Coulomb friction coefficient μ_0	0.3	/
Falling ratio λ [12]	0.2 for falling friction; 0 for constant friction	/
Saturation coefficient κ [12]	0.05	/
Longitudinal creepage	0	/
Spin creepage	0	/
Longitudinal semi-axis of contact ellipse a	4.1	mm
Lateral semi-axis of contact ellipse b	3.1	mm
Normal load	25.8	kN

2.2 Description of the wheel/rail interaction model

The wheel is modelled through a modal approach; mode shapes (ϕ_i) and natural frequencies (ω_i) are extracted from an axisymmetric finite element model of the wheel described in Section 3. At the contact point the interaction with the rail is assumed to excite the wheel in two directions: normal and tangential to the contact plane; the other directions are neglected.

The contact in the normal direction is represented by a linearized contact spring while the lateral forces are modelled through creep forces as described in Section 2.1. Figure 2 shows a schematic representation of the system as considered here. The physical coordinates *x* and *y* are used to represent lateral and vertical directions, while *t* and *n* represent the directions tangential and normal to the contact plane, forming a coordinate system rotated by an angle α with respect to x-y. The angle α represents the direction of the plane tangential to the wheel and rail surfaces at the contact point relative to the horizontal. In this simplified model the rail is assumed to be rigid. The motion of the belt in Figure 2 represents the sliding velocity in the transverse direction due to curving.

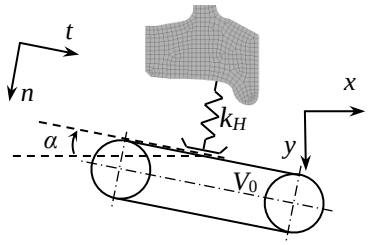

Figure 2. Schematic representation of wheel-contact forces system

For small vibration around the steady-state condition, the equations of motion in modal coordinates are:

$$\mathbf{I}\ddot{\mathbf{q}} + \mathbf{C}_q\dot{\mathbf{q}} + \mathbf{K}_q\mathbf{q} = \mathbf{\Phi}^{\mathbf{T}}\begin{Bmatrix} f_x \\ f_y \end{Bmatrix} = (\mathbf{T}\mathbf{\Phi_0})^{\mathrm{T}}\mathbf{R}\begin{Bmatrix} f_t \\ f_n \end{Bmatrix} \tag{1}$$

where **I** is the identity matrix; the modal damping matrix $\mathbf{C}_q$ and modal stiffness matrix $\mathbf{K}_q$ are diagonal with diagonal terms equal to $2\zeta_i\omega_i$ and ω_i^2 respectively, where ζ_i is the modal damping ratio, while $\mathbf{\Phi_0}$, **T** and **R** are defined as:

$$\mathbf{\Phi_0} = \begin{bmatrix} \Phi_{x1,0} & \Phi_{x2,0} \\ \Phi_{y1,0} & \Phi_{y2,0} \\ \Phi_{rz1,0} & \Phi_{rz2,0} \end{bmatrix}, \mathbf{T} = \begin{bmatrix} 1 & 0 & -\Delta_y \\ 0 & 1 & \Delta_x \end{bmatrix} \text{ and } \mathbf{R} = \begin{bmatrix} \cos\alpha & \sin\alpha \\ -\sin\alpha & \cos\alpha \end{bmatrix} \tag{2}$$

Here $\phi_{x1,0}$, $\phi_{x2,0}$ are the mode shapes in the x direction evaluated at the nominal contact point; $\phi_{y1,0}$, $\phi_{y2,0}$ are the mode shapes in the y direction; $\phi_{rz1,0}$, $\phi_{rz2,0}$ are the rotational displacements in these modes about the longitudinal direction (with clockwise taken as positive). Δ_x is the lateral offset, i.e. the distance between the nominal contact point and the actual one, while Δ_y is the vertical offset. Therefore $\mathbf{\Phi} = \mathbf{T}\mathbf{\Phi_0}$ represents the mode shapes evaluated at the actual contact point considered in the simulation. **R** represents a rotation

matrix to transform the dynamic forces from directions tangential and normal to the contact (f_t and f_n) into the *x* and *y* directions.

The modal coordinate transformation is defined as

$$\mathbf{q} = \mathbf{\Phi}^{\mathbf{T}} \begin{Bmatrix} u_x \\ u_y \end{Bmatrix} \tag{3}$$

with u_x and u_y representing the dynamic displacements at the contact point in the x and y directions. The forces in the right-hand term in Eq.(1) are themselves dependent on the displacement and velocity at the contact point and will constitute the coupling between the modes considered.

In the normal direction n, linearized Hertz contact theory can be applied for small amplitudes of displacement [1]. The dynamic component of the normal force f_n can be expressed through the contact stiffness as:

$$f_n = -k_H u_n \tag{4}$$

where u_n is the dynamic displacement in the normal direction and k_H is the linearized Hertz contact stiffness in the normal direction.

The creep force is calculated as the product of the adhesion coefficient μ and the normal force N. In general the adhesion coefficient itself depends on both the sliding velocity and the normal load [33] but the dependence on the normal load is neglected. By writing the friction force $f_{t,tot}$ as a sum of a steady-state part $f_{t,0}$ and a dynamic part, the dynamic component of the creep force f_t can be found from:

$$f_t = f_{t,\mathrm{tot}} - f_{t,0} = \mu\left(\gamma_0 + \frac{v_t}{V}\right)(N_0 + f_n) - \mu(\gamma_0)N_0 \tag{5}$$

where the subscript 0 denotes the quasi-static quantities evaluated at the steady-state condition. V is the rolling velocity and v_t is the vibration velocity in the tangential direction. The quasi-static lateral creepage γ_0 also corresponds approximately to the angle of attack (or yaw angle) of the wheel relative to the rail. Previous studies have shown that squeal occurrences are dependent on angle of attack (see e.g.[15, 31]). In this modelling approach, however, if constant friction is considered and the angle of attack is large enough for the creep-adhesion curve to be in the saturated region, the actual value of the angle of attack is no

longer important for stability. When including falling friction, the angle of attack is important in the whole creepage range as it affects the slope of the friction curve.

For the purpose of analysing the response of the system in the frequency domain, the friction force can be linearized around the steady-state condition. This only allows the prediction of linearized instability, while the nonlinear limit cycle will be addressed separately below. The friction force linearized around the steady-state condition is given by:

$$f_t \cong \mu(\gamma_0) f_n + \frac{\partial \mu}{\partial \gamma_0}\frac{N_0}{V} v_t \tag{6}$$

Introducing a modal coordinate transformation, the dynamic force vector becomes:

$$\begin{aligned} \begin{Bmatrix} f_t \\ f_n \end{Bmatrix} &= \begin{Bmatrix} \frac{\partial \mu}{\partial \gamma_0}\frac{N_0}{V} \\ 0 \end{Bmatrix} v_t + \begin{Bmatrix} (-\mu(\gamma_0) k_H) \\ -k_H \end{Bmatrix} u_n \\ &= \begin{bmatrix} \frac{\partial \mu}{\partial \gamma_0}\frac{N_0}{V} & 0 \\ 0 & 0 \end{bmatrix} \mathbf{R}^{\mathrm{T}} \mathbf{\Phi} \dot{\mathbf{q}} + \begin{bmatrix} 0 & -\mu(\gamma_0) k_H \\ 0 & -k_H \end{bmatrix} \mathbf{R}^{\mathrm{T}} \mathbf{\Phi} \mathbf{q} \end{aligned} \tag{7}$$

Then the right hand term of Eq.(1) becomes:

$$\begin{aligned} \mathbf{\Phi^{\mathrm{T}}} \begin{Bmatrix} f_x \\ f_y \end{Bmatrix} &= \mathbf{\Phi}^{\mathrm{T}} \mathbf{R} \begin{bmatrix} \frac{\partial \mu}{\partial \gamma_0}\frac{N_0}{V} & 0 \\ 0 & 0 \end{bmatrix} \mathbf{R}^{\mathrm{T}} \mathbf{\Phi} \dot{\mathbf{q}} + \mathbf{\Phi^{\mathrm{T}}} \mathbf{R} \begin{bmatrix} 0 & -\mu(\gamma_0) k_H \\ 0 & -k_H \end{bmatrix} \mathbf{R}^{\mathrm{T}} \mathbf{\Phi} \mathbf{q} \\ &= \mathbf{C}_{qF} \dot{\mathbf{q}} + \mathbf{K}_{qF} \mathbf{q} \end{aligned} \tag{8}$$

The overall linearized equation of motion can then be formulated as:

$$\mathbf{I}\ddot{\mathbf{q}} + \left(\mathbf{C}_q - \mathbf{C}_{qF}\right)\dot{\mathbf{q}} + \left(\mathbf{K}_q - \mathbf{K}_{qF}\right)\mathbf{q} = 0 \tag{9}$$

where the sizes of the matrices $\mathbf{C}_q$, $\mathbf{C}_{qF}$, $\mathbf{K}_q$, $\mathbf{K}_{qF}$ are $N_m \times N_m$ where N_m is the number of modes considered in the model. For all calculations presented in this paper, for clarity, only two modes are considered and the effect of other modes is neglected.

3 Description of the parameters of cases studied

The wheel considered in this study is a resilient wheel from a tram, shown in Figure 3. A Finite Element (FE) model of this wheel was developed and validated in [13] and has been adopted here. The modal damping ratios have been obtained from measurements, while the

parameters representing the rubber elements in the FE model have been updated so that the natural frequencies match those found in the measured data (see [27]). The radial and axial mobilities of this wheel at the nominal contact point are shown in Figure 4, in which the FE results (after model tuning) are compared with measured data.

Different pairs of modes from this wheel are selected for analysis. To select the pairs of modes, some preliminary calculations have been performed by making use of the more complete curve squeal model developed by Huang [12]. With this more complete model, the stability of the system with a constant friction coefficient has been studied by using the Nyquist criterion [34] in the frequency domain. The pairs of modes likely to be involved in mode coupling have been identified by running the model again while including only these modes in the modal basis of the wheel. If the corresponding unstable frequencies remain, the selected pairs of modes are identified to be those involved in squeal.

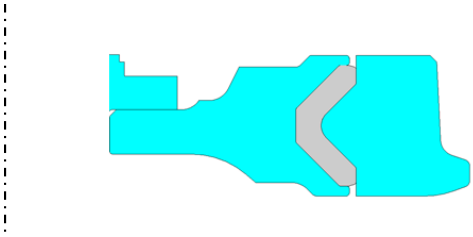

Figure 3. Cross-section for a resilient tram wheel, radius 330 mm.

Among the pairs of modes found to be unstable two, related to measured squeal frequencies, have been selected (Table 2). The mode shapes of the chosen modes and their vector representations at the nominal contact point are shown in Figure 5. To describe the wheel modes, the number of nodal diameters *n* and the number of nodal circles *m* are used. For the mode at 2536 Hz the presence of the rubber layer in the resilient wheel makes it more difficult to assign a simple description to the mode shape based on nodal diameters and nodal circles. With the normalisation applied in the FE model the modal masses of the selected modes are all equal to 0.5 kg.

Table 2. Parameters of two-mode model used for different cases

		(*n*,*m*)	Natural frequency (Hz)	Mode shape at nominal contact point (normal direction) (m)	Mode shape at nominal contact point (axial direction) (m)	Rotation mode shape about longitudinal direction (rad)	Original Damping ratio
Case 1	Lower mode	(4, 1)	2474	-6.8×10^{-2}	-1.1×10^{-1}	-9.5×10^{-1}	4.2×10^{-3}
	Higher mode	*n* =1; See Figure 5	2536	1.5×10^{-2}	7.9×10^{-2}	3.5×10^{0}	5.9×10^{-3}
Case 2	Lower mode	(3, 0)	1271	6.0×10^{-2}	-1.0×10^{-1}	-7.2×10^{-1}	7.2×10^{-3}
	Higher mode	(3, 1)	1417	-8.7×10^{-2}	-8.0×10^{-2}	-6.4×10^{-1}	1.2×10^{-2}

In all the calculations performed for this paper, the wheel is assumed to be the left wheel of a leading wheelset of a bogie, while the curve can be a left-hand or right-hand curve depending on whether the inner or outer wheel is considered. For the left wheel, the contact angle is assumed to be always positive (see Figure 2); the steady-state creepage is always positive for a right-hand curve and negative for a left-hand curve.

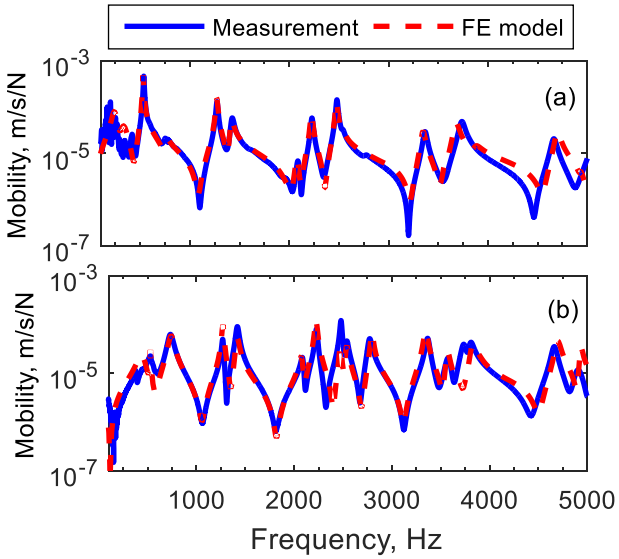

Figure 4. Tram wheel mobilities at nominal contact point. (a) Axial direction; (b) radial direction

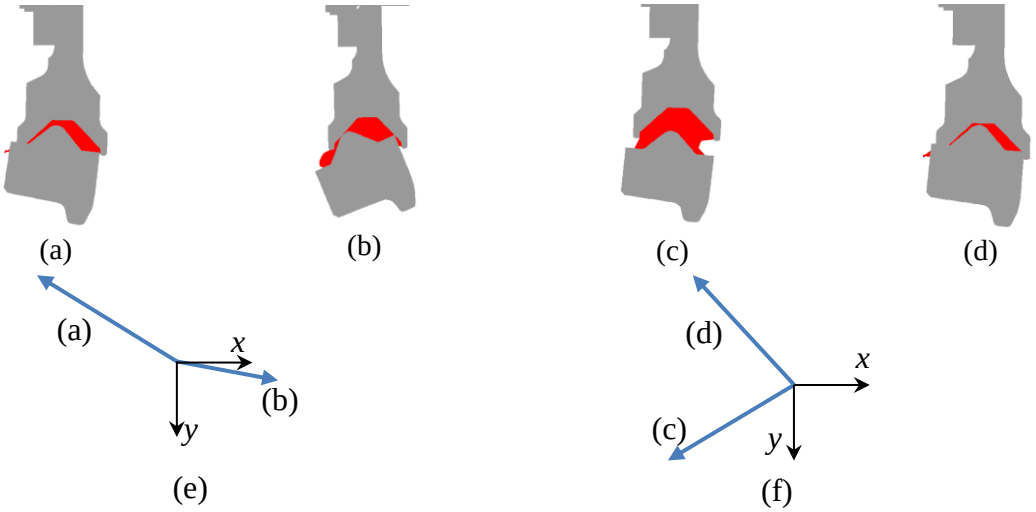

Figure 5. Mode shapes of resilient tram wheel (a) *n*=4 at 2476 Hz; (b) *n*=1 at 2536 Hz; (c) *n*=3 at 1271 Hz; (d) *n*=3 at 1417 Hz; (e) mode shape vectors for modes (a), (b); (f) mode shape vectors for modes (c) and (d) at nominal contact point

4 Frequency-domain results from two-mode model

Results from the frequency domain model are shown in this section by evaluating the real part of the eigenvalues; positive values indicate instability. Results are presented as a function of the quasi-static adhesion coefficient $\mu(\gamma_0)$, as well as the lateral offset of the contact position Δ_x, the contact angle α, the damping ratio ζ_i and the slope of the friction curve. Although these parameters are not completely independent of each other, they are assessed here independently to give a more complete overview of their effect on the stability of the system described in Eq. (9). A constant friction model is assumed throughout this section, except for the case devoted to analysing the slope of the friction curve.

4.1 Effect of the adhesion coefficient on stability and unstable frequency

First, an example is presented for each of the two cases to show the effect of the adhesion coefficient on the stability. For Case 1, a left-hand curve is considered (the wheel is the inner wheel) and the contact point is assumed to be on the wheel tread with an offset of 10 mm towards the flange. Figure 6 shows the results. For a friction coefficient of 0.53 one of the two eigenvalues becomes positive and the system is unstable. The imaginary parts, which when converted into Hz correspond to the frequency of oscillation, start at certain values and become closer with increasing adhesion coefficient. From the imaginary part of the eigenvalue the corresponding unstable frequency is found to be 2534 Hz.

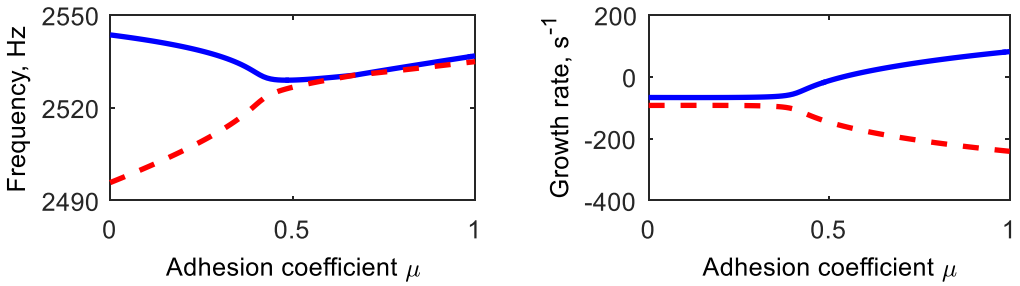

Figure 6. Imaginary part (frequency) and real part (growth rate) for Case 1

For Case 2, the imaginary part and the real part of the eigenvalues of this system are shown in Figure 7 for a right-hand curve (the wheel is an outer one), with an offset of 20 mm and a contact angle of 20˚. Instability occurs for adhesion coefficients above about 0.6 when the real part of one eigenvalue increases to be larger than zero. The imaginary parts at $\mu = 0$ are higher than the natural frequencies of the two modes (1271 Hz and 1417 Hz); this is due to the vertical contact stiffness k_H in $\mathbf{K}_{qF}$ in Eq. (8). The squeal frequency is predicted to be around 1470 Hz.

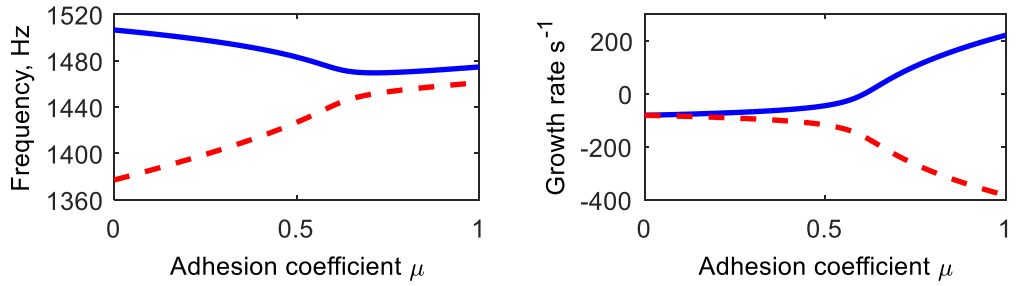

Figure 7. Imaginary part (frequency) and real part (growth rate) for Case 2

4.2 Combined effect of the adhesion coefficient and lateral offset

In this section, the effect of varying the lateral contact position is determined for a left-hand curve (the wheel is the inner wheel) with the contact point assumed to be on the wheel tread. The contact angle is assumed to remain constant at 3˚ according to the wheel section design. The nominal contact point is defined as 0 mm. A negative offset means that the contact point moves away from the flange. A stability analysis is performed by studying the sign of the real parts of the eigenvalues (growth rate).

The results for Case 1 are presented in Figure 8 in the form of a stability map. The adhesion coefficient μ is varied between 0 and 1. The stability map is divided into stable and unstable areas by studying the sign of the real part of the eigenvalues of Eq. (9). Instability can be found for this case only for positive offsets although there are other pairs of modes that are

unstable for negative offsets. For Case 2 the system was found to be stable for any contact position across the wheel tread.

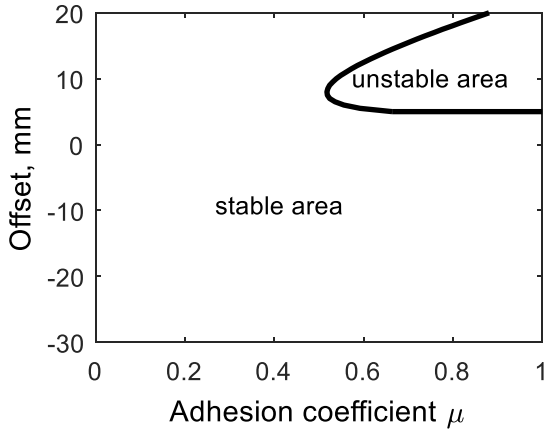

Figure 8. Stability map for the inner wheel for contact on the tread. Effect of the offset of the contact point from the nominal position and of the adhesion coefficient: Case 1.

4.3 Combined effect of the adhesion coefficient and contact angle

To study the effect of the contact angle, the wheel is assumed to be traversing a right-hand curve (i.e. it is the outer wheel) and the contact point is assumed to be on the flange. For simplicity, the offset is assumed to remain constant as 20 mm with the contact position at the middle of the flange, whilst the contact angle is varied between 0˚ and 90˚. The rotation of the contact plane is implemented by means of a rigid rotation from *x*-*y* to *n*-*t* coordinates as shown in Figure 2. Clearly, the range of rotations considered is exaggerated compared with railway applications but it allows the instability trends to be captured in a wider area.

Again the adhesion coefficient μ is varied between 0 and 1. The corresponding stability maps are shown in Figure 9. Instability is found for Case 2 while Case 1 is always stable. The pair of modes at 1.2 and 1.4 kHz can lead to instability below 30˚ with adhesion coefficients above 0.6. Often curve squeal is attributed to the inner wheels but these findings confirm that the outer wheel may also squeal and mode coupling is a possible mechanism behind this phenomenon. The modes involved are not necessarily the same as for the inner wheel.

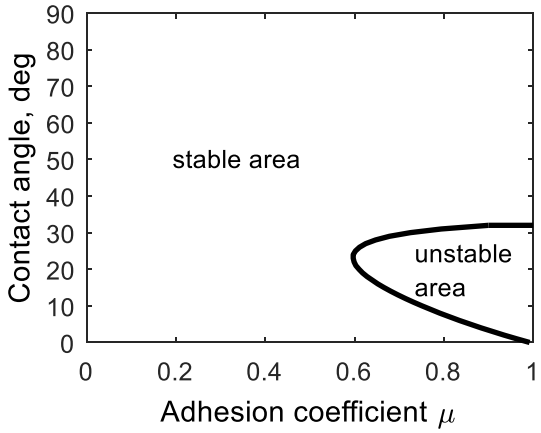

Figure 9. Stability maps for the outer wheel for contact on the flange. Effect of the contact angle and of the adhesion coefficient: Case 2

The effect of additional modes on the stability maps has also been investigated by introducing one at a time modes close in frequency to those considered. Results are not reported here for brevity but show that the stability maps are only marginally affected by introducing more than two modes in the analysis.

4.4 Effect of wheel damping

Increased wheel damping is often proposed as a solution for curve squeal, although in practice it is not always found to be successful [5]. In this section, the same two cases are adopted to discuss the effect of changing the damping ratios of the two modes. For Case 1, contact on the wheel tread is considered with an offset of 10 mm, therefore in the unstable region shown in Figure 8. For Case 2, flange contact is considered and a single contact angle of 10˚ is used, which is in the unstable region shown in Figure 8.

First, the damping of the higher frequency mode of each pair is varied between 10^{-4} and 10^{-1} while the damping of the lower frequency mode is kept constant and equal to the original value shown in Table 2. Figure 10 shows the corresponding stability maps. For Case 1, increasing the damping ratio of the higher frequency mode always has a beneficial effect in terms of the stability of the system. For Case 2, however, the stability is marginally dependent on damping and there is a range of damping ratios in which increasing the damping can make the system slightly more unstable. When the damping ratio of the lower frequency mode is changed, it is found that the stability maps are similar to these results so they are not shown here.

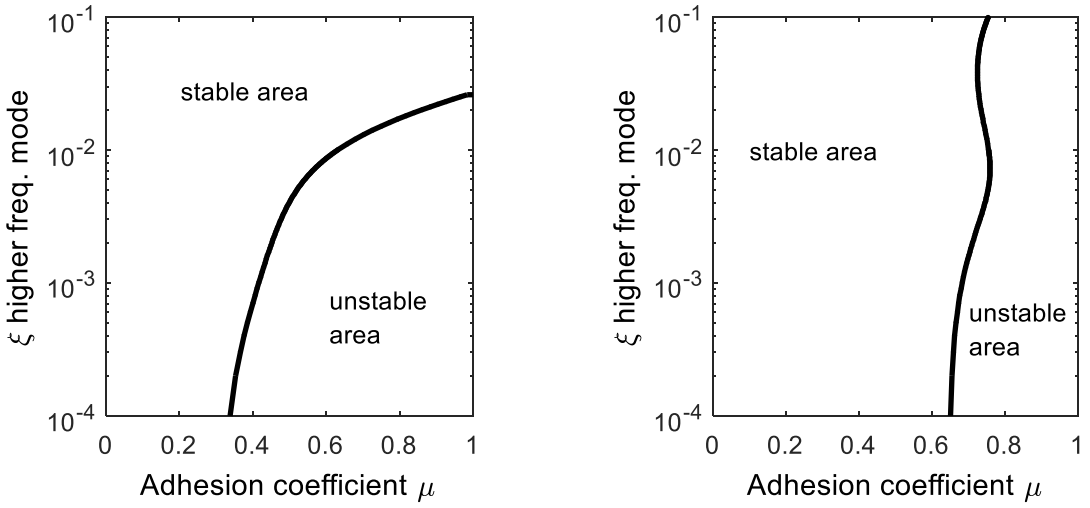

Figure 10. Effect of changing the damping ratio of the higher frequency mode. (a) Case 1, 10 mm offset; (b) Case 2, contact angle 10˚.

The effect of changing the damping of both modes simultaneously is shown in Figure 11. These are plotted against the damping ratio of the higher frequency mode while the ratio of the two damping ratios (ξ_1/ξ_2) is kept constant. As before the stable areas are always to the left of the corresponding lines. The results for both cases have the same trend. For values of damping below a certain limit, the stability of the system is not affected by changes in the damping ratios. This limit value is different for the two cases, being as low as 0.1% for Case 1 and around 0.8% for Case 2.

In summary, adding damping to the wheel does not automatically eliminate the possibility of curve squeal. If the mechanism responsible for the instability is mode coupling, in the extreme case that the damping of a single mode is increased, the system can even become more unstable in certain situations. This behaviour has been observed previously by other authors and has often been described as the "destabilisation paradox", see e.g. [35]. Even for a more realistic case where the damping is increased for both modes, a limit value needs to be exceeded for the added damping to have a significant effect in eliminating the instability.

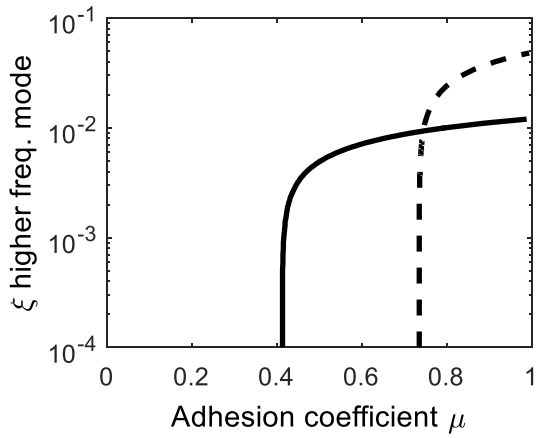

Figure 11. Effect of damping (keeping the ratio between the two modes ζ_1/ζ_2 constant). Solid line: Case 1, 10 mm offset; dash line: Case 2, contact angle 10˚.

4.5 Effect of friction curve slope

If a falling region is introduced in the friction model, the damping of the system is modified by the friction force. With a single-mode model of the wheel, a limit value of the friction slope for stability can be calculated. According to [14], this can be found as:

$$\frac{\partial \mu}{\partial \gamma_0} = \frac{2\omega_i \xi_i V}{N\Phi_{xi}^2} \tag{10}$$

where Φ_{xi} is the mass-normalised mode shape in the tangential direction of the i^{th} mode. However, for a two-mode system this simple estimate no longer applies.

To show the effect of friction slope, Case 2 is considered here and the maximum friction coefficient μ_0 is set to equal to 0.8. The stability map with different friction slopes and contact angles is shown in Figure 12. The solid line shows the division between stable and unstable areas for the two-mode system. As shown already in Figure 9 the system with constant friction is unstable at this value of friction coefficient between about 8° and 30°. Figure 12 also shows the minimum friction slopes that would result in instability when each wheel mode is considered as a single degree of freedom (SDOF) system (i.e. from Eq. (10)) in the axial direction (dashed line and dotted line). For all the curves, the stable region is always below the line and the unstable region is above.

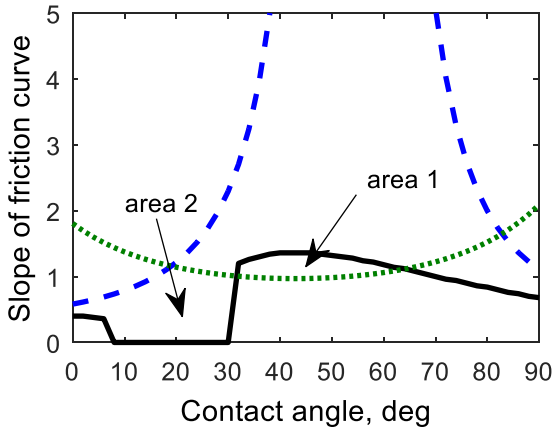

Figure 12. Stability map with different contact angles and friction curve slopes for Case 2 with $\mu = 0.8$ (solid line: mode coupling; dashed line: lower frequency mode; dotted line: higher frequency mode). Stable regions are below the corresponding lines.

In the region above both the solid and dotted/dashed lines the system is considered to be unstable due to the negative slope of the friction curve. Two interesting areas can be identified between the continuous and broken lines. They are highlighted as 'area 1', 'area 2' in the figure. Inside area 1, the two-mode system is stable, although the slope of the friction curve is above the limit value of the lower frequency mode. However, inside area 2, the system is unstable due to mode coupling as the slope of the friction curve is below the limit value for either single mode. The shape of area 2 changes as the slope of the friction curve is increased and this suggests that the negative slope is modifying the damping of the system, and consequently affecting the mode-coupling instability.

5 Time-domain results for two-mode model

To include the nonlinearities of the friction force, in this section time-domain simulations are also carried out for Case 2 by using a step-by-step integration method (Runge-Kutta method [36]). This allows the nonlinearity to be fully considered and the limit cycle to be calculated. The contact angle and friction coefficient are chosen as 20˚ and 0.8 respectively.

Figure 13 shows the time-domain solutions for this two-mode system. The initial conditions given to solve the simulation are 78 N for the dynamic component of the normal force and 460 N for the lateral one. It can be seen that the responses in both tangential and normal directions increase until the limit cycle is reached. The close-up of the limit cycle shows a phase difference between the responses in the two directions. This is another important feature of mode-coupling instability and is necessary for the energy transfer between these

two directions [22]. The spectrum shows that the frequency of the limit cycle is 1496 Hz (from frequency domain analysis it was predicted at around 1470 Hz). This is not equal to either of the natural frequencies of the two modes considered (i.e. 1271 Hz and 1417 Hz); nor does it correspond to the frequency of one of the modes when coupled to the contact stiffness (1377 and 1506 Hz). The higher frequency peaks in the spectrum correspond to higher harmonics due to the non-linearity.

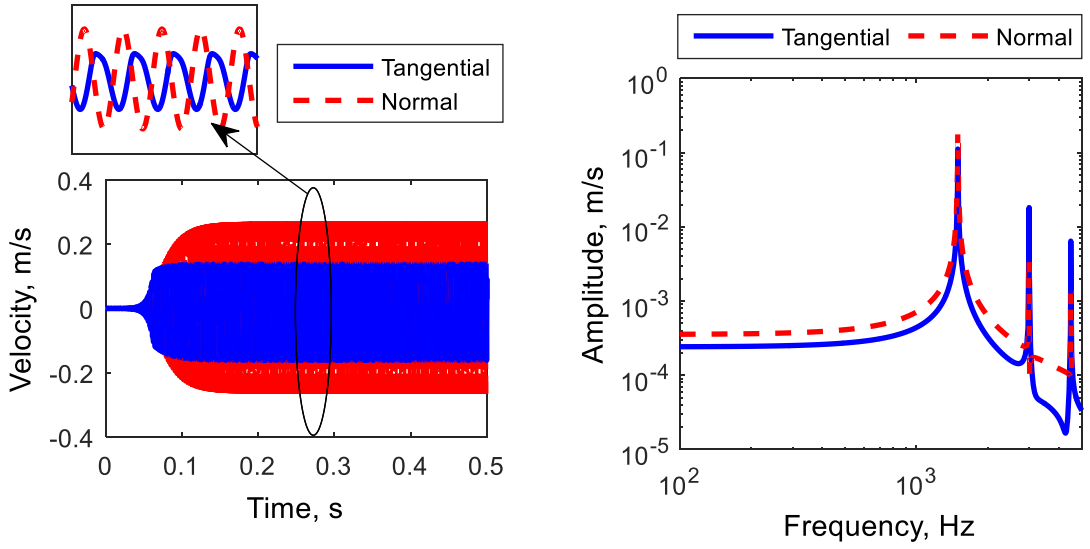

(a) (b)

Figure 13. Time-domain solution for Case 2 with angle of 20˚, friction coefficient of 0.8 and offset of 20mm. (a) Complete solution; (b) spectrum of the responses.

Next, the phase shift is investigated when both mode coupling and falling region are included. Again, Case 2 is adopted and three different combinations of contact angle and adhesion coefficient are used. A falling friction law is considered with different friction curve slopes at the steady-state creepage value.

From the time-domain simulations the phase difference of the limit cycle between the two directions is calculated by taking the Fourier transform of the limit cycle response. The results are shown in Figure 14(a). It can be seen that with larger slopes, the phase difference tends to 0˚. This is aligned with the results shown in Figure 12, where a slope of 2 or more was found to be above the single mode stability lines. In the absence of mode coupling where a single (real) mode is responsible for squeal the phase difference is expected to be zero. Figure 14(b) gives the squealing frequency at the limit cycle; it starts from around 1500 Hz and tends to the frequency of the higher mode (1417 Hz). In the absence of mode coupling the instability is due to negative damping and is associated to a single wheel mode. The presence of a phase difference and frequency shift are indicators of the presence of mode

coupling although they do not exclude falling friction, as both mechanisms may be acting together, as illustrated in Section 4.5.

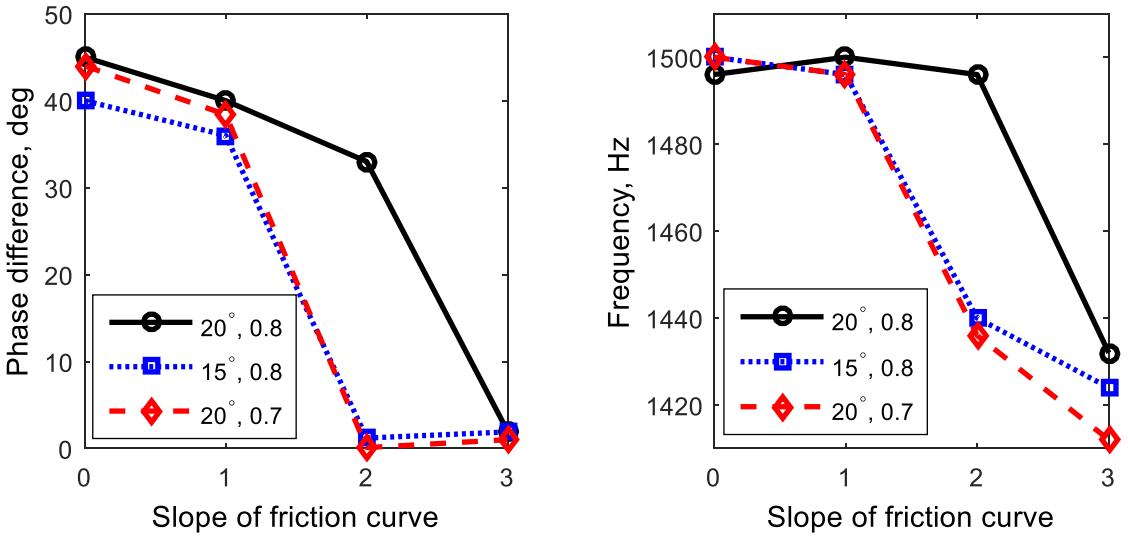

(a) (b)

Figure 14. Phase difference and squealing frequency with different friction slopes for Case 2: (a) phase difference; (b) squealing frequency

6 Frequency shift and phase difference observed in field measurements

The wheel adopted in the calculations above is an example of a resilient wheel used for trams. Some field experiments have been presented in [27] with this type of wheel running on a curve with severe squeal noise problems. The selected test section had a very small curve radius of 18 m with grooved rails and ballasted track; as a result the angle of attack was large and found to be around 2.5˚ [13] and it can be fully expected that the contact is in the saturated region. The wheel was fitted with accelerometers and vibration data were recorded in both axial and radial directions on the wheel tyre. The wheel vibration measurements can provide some useful understanding in analysing the possible mechanism behind curve squeal and results are presented here to allow a qualitative comparison with the models described above.

An example of the measured wheel vibration is shown in Figure 15. In this example the instrumented wheel was the front inner one and the tram running speed was 2.78 m/s. It can be seen that the wheel vibrates at a relatively high level in the time period from about 13 s to 25 s. From the spectrograms, it is found that there are two dominant frequencies for both axial and radial directions. They are around 1.5 kHz and 2.5 kHz and these broadly

correspond to the squealing frequencies in the cases analysed above. A peak is also present around 3.7 kHz.

A close-up plot of part of the acceleration signal from Figure 15 is shown in Figure 16 along with the corresponding frequency spectra. The most important features of squeal are evident, with the vibration being intermittent, mono-tonal and of very high levels. The squealing frequency in this time window is at 2517 Hz, as shown in Figure 16(b).

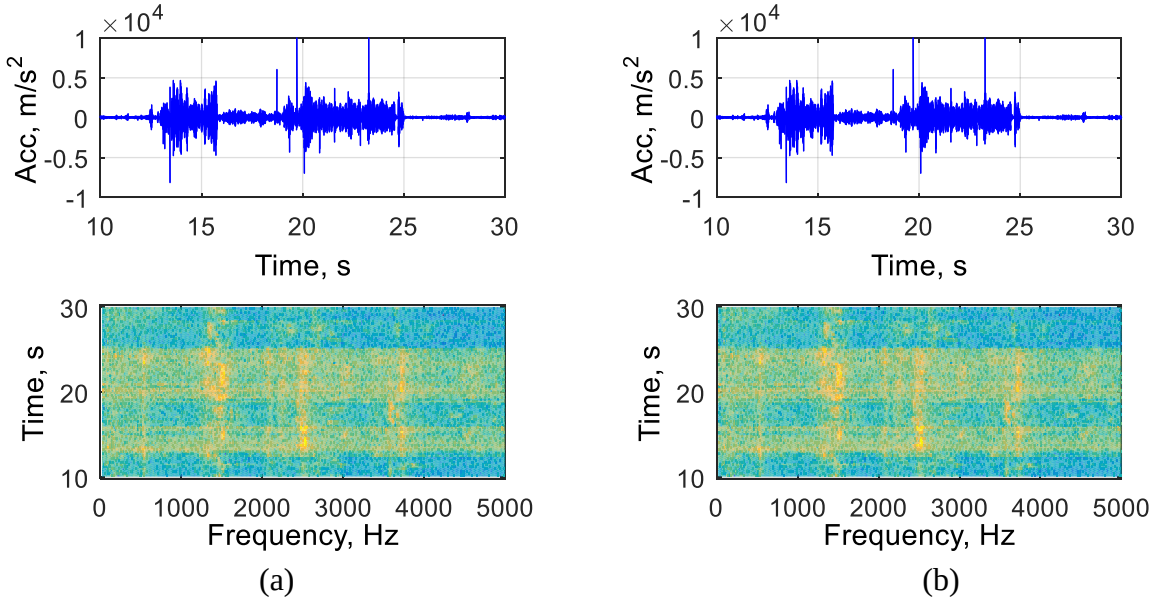

Figure 15. Wheel vibration acceleration measured and their spectrograms: (a) axial direction; (b) radial direction.

At around this frequency this wheel has the two vibration modes included in Case 1 above and it has been shown that for an offset of around +5 mm mode coupling instability can arise (Figure 8). In addition, as shown in Section 5, another important feature of mode coupling is a phase lag between the radial and axial vibration. Figure 16(a) shows an additional close-up plot of the vibration data showing a phase lag of about 20˚ between the two directions.

An additional example is shown in Figure 17. The squealing frequency is 1515 Hz and does not correspond to any of the modes in Figure 4, the nearest measured natural frequencies being at 1271 and 1414 Hz; this is similar to the results found in Sections 4 and 5. Again there is a phase lag of about 30˚ between the two directions that qualitatively resembles the one obtained with the model in Figure 13(a).

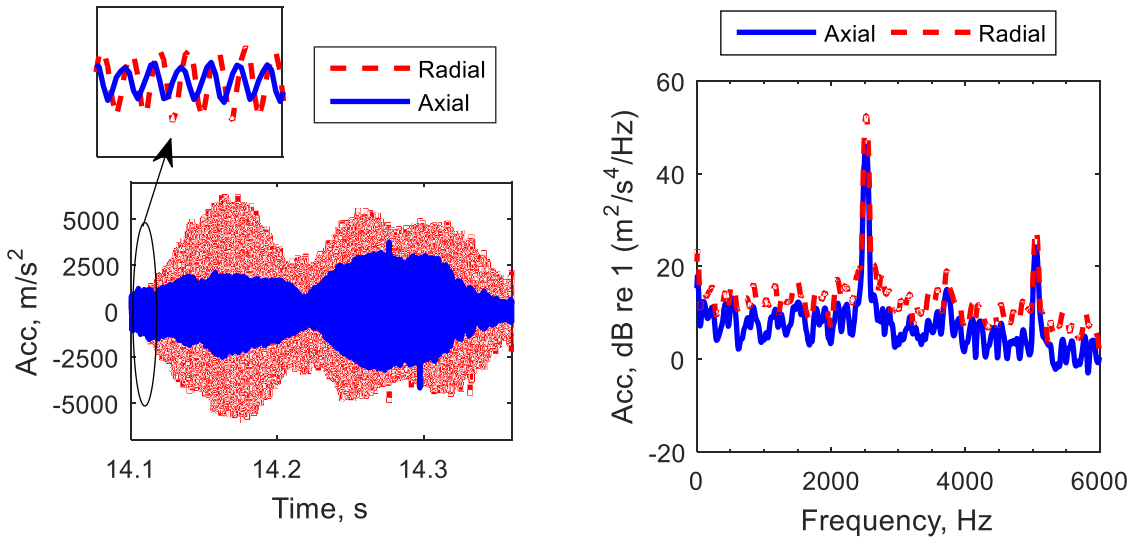

(a) (b)

Figure 16. Wheel vibration measured during squeal at 2522 Hz. (a) Example of time history data (b) frequency spectrum.

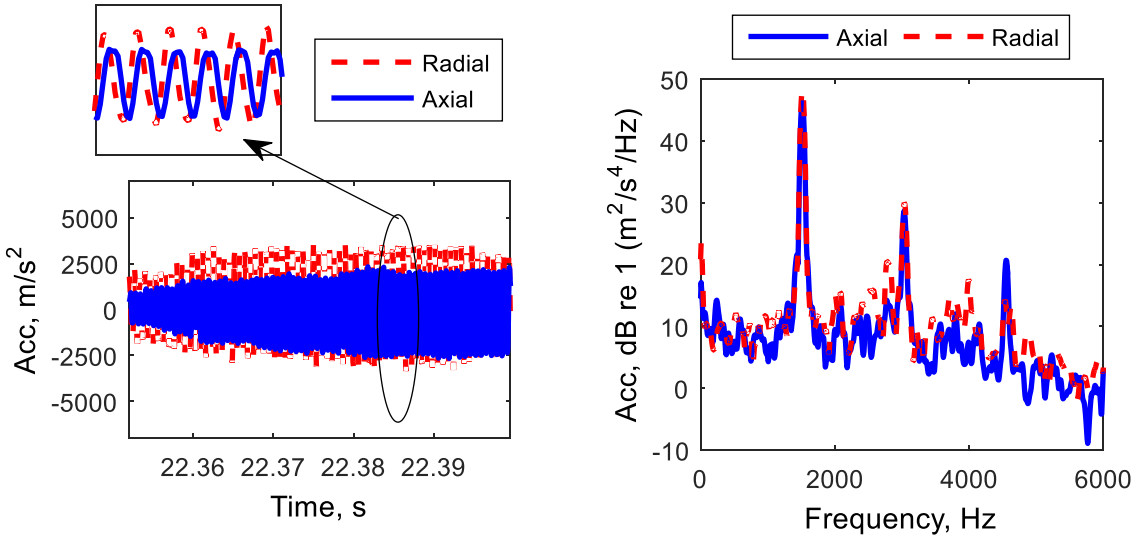

(a) (b)

Figure 17. Wheel vibration during squeal at 1515 Hz. (a) time data and (b) frequency spectrum.

The measurement data shown here therefore include two important characteristics of mode coupling: the squealing frequency is different from the natural frequencies of the modes involved and there is a phase lag between the radial and axial directions. Both features have also been found in this paper with the model with constant friction.

The wheel acceleration data from a number of pass-bys have been analysed statistically to determine the distribution of the squealing frequency and the phase difference between the axial and radial directions. Three main squealing frequencies were observed, at around 1.5,

2.5 and 3.7 kHz as seen in Figure 15. The phase difference has been calculated at every oscillation period after applying a band-pass filter around the squealing frequency. Only those time windows with vibration levels above 800 m/s^2 (rms) have been selected to compute the phase difference. The average squealing frequencies were calculated over the same cycles and found to be 1489 Hz, 2514 Hz and 3713 Hz with standard deviations of 47 Hz, 21 Hz and 48 Hz.

A summary of the measured phase difference for these three squealing frequencies is shown in Figure 18. The horizontal axis represents the absolute value of the phase difference in degrees while the vertical axis indicates the number of times the difference occurs in a certain 10˚ range. To obtain these results three different pass-bys at 10 km/h have been considered. It can be seen that the phase difference can vary between 0˚ and 180˚ with the greatest tendency for the phase differences to be in the range between 10˚~40˚ and 120˚~160˚, especially for the squealing frequency of 1489 Hz. This broadly agrees with the results from the model in Figure 14 for small values of friction slope.

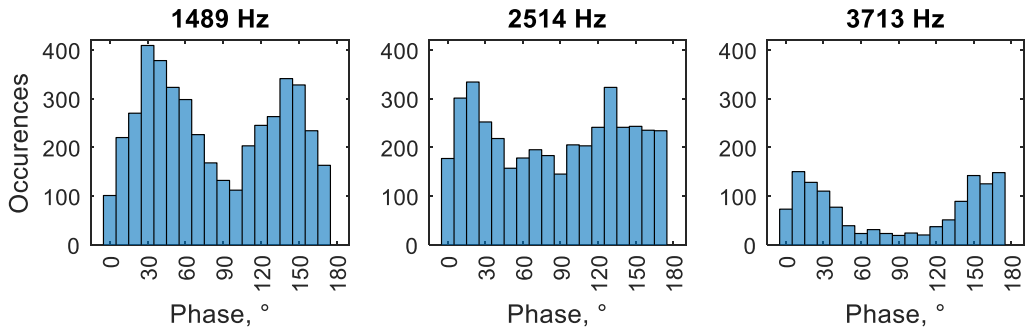

Figure 18. Phase difference for three squealing frequencies.

The experimental results therefore show the same features as the model. The squealing frequencies of 1489 Hz and 2514 Hz are similar to those found in Section 4 and the non-zero phase difference corresponds to that found for the case of mode coupling. There are too many uncertainties in the measurement campaign to allow a full quantitative comparison between the model and measurements. In particular, it was not possible to determine the actual friction coefficient or the exact contact position. Nevertheless, the evidence presented here gives additional indications that mode coupling is a possible mechanism behind curve squeal at least in some situations.

7 Conclusions

A two-mode model has been used to illustrate the features of the mode-coupling mechanism, which can be a cause of curve squeal noise in addition to the traditional falling friction mechanism.

By carrying out a parametric study using frequency-domain stability analysis, it is shown that the offset and the contact angle can both have an effect on the squeal noise. This confirms that both inner and outer wheels in the curve can result in squeal noise due to mode coupling. Moreover, it is shown that the damping ratio can play an important role. Increasing the damping of a single mode does not always have a beneficial effect on squeal noise and in some cases can actually make the system more prone to squeal. Increasing the damping of both modes simultaneously has no effect until a certain limit is reached. For the wheel modes studied here this limit on the damping ratio is found to be between 0.1% and 0.8%. The effects of the negative slope and mode coupling are also investigated together. Compared with the stability of a single vibration mode, in some situations instability occurs at lower levels of friction slope but in other situations at higher levels.

By analysing the system in the presence of a mode-coupling instability, it is demonstrated that a difference can exist between the squealing frequency and the natural frequency of the wheel modes. Moreover by studying the time-domain response, a phase difference is observed between the vertical and lateral vibration which is a characteristic of mode coupling. If a negative friction slope is gradually included in the model this phase shift decreases and tends to vanish once the negative slope mechanism becomes dominant.

Finally, some results from field measurements of wheel acceleration have been presented. Measured data show similar characteristics to those that were attributed to mode coupling in the modelling, as both frequency and phase shift are detected in the wheel signals. These qualitative comparisons provide additional indications that mode coupling is a possible mechanism for curve squeal.

All data published in this paper are openly available from the University of Southampton repository at https://doi.org/10.5258/SOTON/D0421.

Acknowledgements

This research was partly funded by the China Scholarship Council (CSC).

References

[1] D.J. Thompson, Railway Noise and Vibration: Mechanisms, Modelling and Means of Control, 1st ed., Elsevier: Oxford, 2009.

[2] A. Wickens, Fundamentals of rail vehicle dynamics, CRC Press, 2005.

[3] J.J. Kalker, Three-dimensional elastic bodies in rolling contact, Springer Science & Business Media, 2013.

[4] F.P. Bowden, D. Tabor, The friction and lubrication of solids, Oxford University Press, Oxford, 2001.

[5] D.J. Thompson, G. Squicciarini, B. Ding, L. Baeza, A state-of-the-art review of curve squeal noise: phenomena, mechanisms, modelling and mitigation, in: 12th International Workshop on Railway Noise, Terrigal, Australia, 2016.

[6] M.J. Rudd, Wheel/rail noise—Part II: Wheel squeal, Journal of Sound and Vibration, 46 (1976) 381-394.

[7] U. Fingberg, A model of wheel-rail squealing noise, Journal of Sound and Vibration, 143 (1990) 365-377.

[8] F. Périard, Wheel-Rail Noise Generation: Curve Squealing by Trams, PhD Thesis, Technische Universiteit Delft, 1998.

[9] M.A. Heckl, I.D. Abrahams, Curve squeal of train wheels, Part 1: mathematical model for its generation, Journal of Sound and Vibration, 229 (2000) 669-693.

[10] M.A. Heckl, Curve squeal of train wheels, Part 2: which wheel modes are prone to squeal?, Journal of Sound and Vibration, 229 (2000) 695-707.

[11] F.G. de Beer, M.H.A. Janssens, P.P. Kooijman, Squeal noise of rail-bound vehicles influenced by lateral contact position, Journal of Sound and Vibration, 267 (2003) 497-507.

[12] Z. Huang, Theoretical Modelling of Railway Curve Squeal, PhD Thesis, University of Southampton, UK, 2007.

[13] G. Squicciarini, S. Usberti, D. Thompson, R. Corradi, A. Barbera, Curve squeal in the presence of two wheel/rail contact points, in: D.A. J. Nielsen, P.-E. Gautier, M. Iida, J. Nelson, T. Tielkes, D. Thompson, D. Towers, P. de Vos (Ed.) Noise and Vibration Mitigation for Rail Transportation Systems, Springer, 2015, pp. 603-610.

[14] O. Chiello, J.B. Ayasse, N. Vincent, J.R. Koch, Curve squeal of urban rolling stock—Part 3: Theoretical model, Journal of Sound and Vibration, 293 (2006) 710-727.

[15] A.D. Monk-Steel, D.J. Thompson, F.G. de Beer, M.H.A. Janssens, An investigation into the influence of longitudinal creepage on railway squeal noise due to lateral creepage, Journal of Sound and Vibration, 293 (2006) 766-776.

[16] S.S. Hsu, Z. Huang, S.D. Iwnicki, D.J. Thompson, C.J.C. Jones, G. Xie, P.D. Allen, Experimental and theoretical investigation of railway wheel squeal, Proceedings of the Institution of Mechanical Engineers, Part F: Journal of Rail and Rapid Transit, 221 (2007) 59-73.

[17] X. Liu, P.A. Meehan, Investigation of the effect of lateral adhesion and rolling speed on wheel squeal noise, Proceedings of the Institution of Mechanical Engineers, Part F: Journal of Rail and Rapid Transit, 227 (2013) 469-480.

[18] X. Liu, P. Meehan, Investigation of the effect of relative humidity on lateral force in rolling contact and curve squeal, Wear, 310 (2014) 12-19.

[19] X. Liu, P. Meehan, Investigation of squeal noise under positive friction characteristics condition provided by friction modifiers, Journal of Sound and Vibration, 371 (2016) 393-405.

[20] J.R. Koch, N. Vincent, H. Chollet, O. Chiello, Curve squeal of urban rolling stock—Part 2: Parametric study on a 1/4 scale test rig, Journal of Sound and Vibration, 293 (2006) 701-709.

[21] C. Collette, Importance of the Wheel Vertical Dynamics in the Squeal Noise Mechanism on a Scaled Test Bench, Shock and Vibration, 19 (2012) 145-153.

[22] N. Hoffmann, M. Fischer, R. Allgaier, L. Gaul, A minimal model for studying properties of the mode-coupling type instability in friction induced oscillations, Mechanics Research Communications, 29 (2002) 197-205.

[23] J.F. Brunel, P. Dufrénoy, M. Naït, J.L. Muñoz, F. Demilly, Transient models for curve squeal noise, Journal of Sound and Vibration, 293 (2006) 758-765.

[24] C. Glocker, E. Cataldi-Spinola, R.I. Leine, Curve squealing of trains: Measurement, modelling and simulation, Journal of Sound and Vibration, 324 (2009) 365-386.

[25] A. Pieringer, A numerical investigation of curve squeal in the case of constant wheel/rail friction, Journal of Sound and Vibration, 333 (2014) 4295-4313.

[26] N. Vincent, J.R. Koch, H. Chollet, J.Y. Guerder, Curve squeal of urban rolling stock—Part 1: State of the art and field measurements, Journal of Sound and Vibration, 293 (2006) 691-700.

[27] R. Corradi, P. Crosio, S. Manzoni, G. Squicciarini, Experimental investigation on squeal noise in tramway sharp curves, in: Proceedings of the 8th International Conference on Structural Dynamics, EURODYN 2011, Leuven, 2011.

[28] D. Fourie, P. Gräbe, S. Heyns, R. Fröhling, Experimental characterisation of railway wheel squeal occurring in large-radius curves, Proceedings of the Institution of Mechanical Engineers, Part F: Journal of Rail and Rapid Transit, Published online (2015).

[29] J. Jiang, R. Dwight, D. Anderson, Field Verification of Curving Noise Mechanisms, in: T. Maeda, P.-E. Gautier, C. Hanson, B. Hemsworth, J. Nelson, B. Schulte-Werning, D. Thompson, P. de Vos (Eds.) Noise and Vibration Mitigation for Rail Transportation Systems, Springer Japan, 2012, pp. 349-356.

[30] J. Jiang, D.C. Anderson, R. Dwight, The Mechanisms of Curve Squeal, in: J. Nielsen, D. Anderson, P.-E. Gautier, M. Iida, J. Nelson, D. Thompson, T. Tielkes, D. Towers, P. de Vos (Eds.) Noise and Vibration Mitigation for Rail Transportation Systems, Springer Berlin Heidelberg, 2015, pp. 587-594.

[31] J. Jiang, D. Hanson, B. Dowell, Wheel Squeal: Insights from Wayside Condition Monitoring, in: 12th International Workshop on Railway Noise, Australia, 2016.

[32] J. Kalker, A fast algorithm for the simplified theory of rolling contact, Vehicle System Dynamics, 11 (1982) 1-13.

[33] A. Monk-Steel, D.J. Thompson, Models for railway curve squeal noise, in: VIII International Conference on Recent Advances in Structural Dynamics, Southampton,UK, 2003.

[34] J.F. Barmanj, J. Katzenelson, A generalized Nyquist-type stability criterion for multivariable feedback systems, International Journal of Control, 20 (1974) 593-622.

[35] L. Charroyer, O. Chiello, J.-J. Sinou, Parametric study of the mode coupling instability for a simple system with planar or rectilinear friction, Journal of Sound and Vibration, 384 (2016) 94-112.

[36] J.C. Butcher, Numerical methods for ordinary differential equations, Third ed., John Wiley & Sons, UK, 2016.